



Chiral surface networks of 3-HPLN – A molecular analog of rounded triangle assembly



J. Hooper^a, D.A. Kunkel^b, S. Simpson^c, S. Beniwal^b, A. Enders^{b,*}, E. Zurek^{c,*}

^a Department of Theoretical Chemistry, Faculty of Chemistry, Jagiellonian University, 30-060 Krakow, Poland

^b Dept. of Physics and Astronomy, University of Nebraska–Lincoln, 855 N 16th Street, Lincoln, NE 68588, USA

^c Department of Chemistry, State University of New York at Buffalo, Buffalo, NY 14260-3000, USA

ARTICLE INFO

Available online 9 May 2014

Keywords:

Self-assembly
Surface chemistry
Chirality
Scanning tunneling microscopy
Density functional theory
Ferroelectrics

ABSTRACT

The self-assembly of 3-hydroxyphenalenone (3-HPLN) on the Ag(111) surface has been studied with scanning tunneling microscopy and first-principles computations. The prochiral 3-HPLN molecule forms zipper-like chains when deposited on the Ag(111) surface, representing a 2D analog of their arrangement in bulk crystals. Upon annealing, local chiral trimer motifs form and serve as building blocks in extended 2D supramolecular networks not observed in 3D crystals. The extended network is porous and is held together via weak van der Waals interactions. The dispersion forces between trimers suggest that their handedness is overall racemic, but the asymmetric packing of 3-HPLN trimers around the pores leads to a chiral network. The offset alignment of neighboring 3-HPLN molecules in the unit cell resembles the offset between neighboring particles that are seen in the most efficient packings of rounded triangles. Computations illustrate that charge is transferred from the Ag(111) surface to the lowest unoccupied orbital of 3-HPLN, and a number of networks (including a honeycomb, as well as an alternative close-packed arrangement) are investigated.

© 2014 Elsevier B.V. All rights reserved.

1. Introduction

The adsorption and self-assembly of organic molecules on metal surfaces can result in chirality at two dimensional surfaces. One of the reasons why these types of systems are intensely studied is because of their applications towards enantioselective heterogeneous catalysis [1–3]. The chiral binding sites which are created upon surface adsorption offer cheaper and cleaner alternatives to homogeneous enantioselective catalysis [4]. Examples where this approach has proved useful include tartaric acid-modified nickel (for the hydrogenation of β -ketoesters) [5] and cinchona-modified Pt (for the reduction of α -ketoacid derivatives) [6]. Chiral surfaces also offer attractive ways to design smart-coatings, chiral molecular recognition, and non-linear optical devices [1].

An object is chiral in three-dimensions provided that it does not possess any symmetry elements which employ reflection. Two different non-superimposable forms of the object, so-called enantiomers, can exist. The physical and chemical properties of these enantiomers may differ, for example their interaction with circularly polarized light, chemical reactivity, and even taste or smell. The substrate destroys all symmetry elements of the adsorbate which are parallel to the surface plane. Chiral adsorbates at two-dimensional surfaces can be easily identified since they lack mirror-plane or glide-plane symmetry

elements which are perpendicular to the substrate. On the surface it is important to distinguish between chirality at the point group level, and chirality at the space group level [7]. Five chiral point groups can be found, C_n with $n = 1-4, 6$, and five of the seventeen wallpaper groups (or ways to tile the plane) are chiral, p_n where $n = 1-4, 6$. Since in general a system may be racemic at either level, it is important to determine if both enantiomers are present. A globally chiral system is obtained when only one enantiomer is found, otherwise the system is only locally chiral.

Clusters which are locally chiral at the point group level may be formed from molecules which are either chiral or achiral in two dimensions. Examples of the former include the “magic” clusters composed of three 4-fluorostyrene molecules on the Cu(111) surface [8], and hexamers of methanol on Au(111) [9]. On the other hand, the 2D-achiral molecule phenylacetylene self-assembles to form right and left-handed hexameric clusters on Au(111) [10]. An example of chirality at the point group level is the networks of hexaphenylbenzene derivatives observed on Au(111), which are chiral as a result of the asymmetric molecular close-packing within half unit cells [11].

Herein, we study the adsorption of the organic molecule 3-hydroxyphenalenone (3-HPLN) to the Ag(111) surface. The three-dimensional crystal of this molecule is particularly interesting since it behaves as a ferroelectric in the condensed phase [12], as does the related molecule croconic acid [13]. Similar to 3-HPLN, croconic acid forms chiral clusters and networks on Ag(111) [14]. Since 3-HPLN contains both a hydrogen bond donor and acceptor, it can readily form

* Corresponding authors.

E-mail addresses: a.enders@me.com (A. Enders), ezurek@buffalo.edu (E. Zurek).

hydrogen bonded supramolecular architectures. It may also interact with nearby molecules via weaker dispersion or dipolar forces. We have carried out scanning tunneling microscopy experiments, supplemented by extensive first-principles calculations, in order to investigate the intermolecular interactions between monomers of 3-HPLN and their adsorption to the surface. Upon annealing, trimers of 3-HPLN are formed on the surface and these motifs are locally chiral at the point group level. But since configurational entropy is likely to favor a racemic mixture of trimers, when integrated over the entire surface the point group chirality vanishes. The trimers interact with each other via van der Waals forces, and the network which they form is chiral at the space group level. Both left and right handed networks have been observed.

We also discuss our results in light of recent studies concerning the emergence of local chiral domains in 2-D systems comprised of achiral objects that interact with each other via their particle shape only. Mason and co-workers [15] concluded that the local chiral domains which spontaneously emerged in a system of equilateral triangles formed as a result of the rotational entropy of the particles. Shell and Carmichael [16] pointed out that the fabrication process must lead to a slight rounding of the triangles, and illustrated via Monte Carlo simulations that this rounding could be used to explain the chiral symmetry breaking, thereby questioning the role of rotational entropy. The particles considered in these studies, perfect equilateral triangles and those with rounded corners, resemble the trimers of 3-HPLN in our work. We note that even though both models do not consider the subtleties of the intertrimer and surface-adsorbate interactions, they may be applicable to our system.

2. Experimental methods

An Omicron low temperature scanning tunneling microscope, operated under ultra high vacuum at a base pressure $<10^{-10}$ mbar, was used for all experiments. The Ag(111) single crystal substrate was cleaned with repeated cycles of Ar ion sputtering and annealing to approximately 620 °C. The substrate cleanliness was checked through STM imaging. An electrochemically etched W-tip was used for all measurements. 3-hydroxyphenalenone (3-HPLN) with 98% purity, was purchased from Acros Organics. 3-HPLN was thermally evaporated in a home built Knudsen cell evaporator onto the cleaned Ag(111) substrate. Post-deposition annealing procedures varied with the samples, and specific annealing temperatures are found in the results section. All samples were cooled to liquid nitrogen temperature for imaging.

3. Computational methods

The ADF software package [17,18] was used to carry out density functional theory (DFT) calculations on isolated 3-HPLN clusters in the gas phase, and on 3-HPLN adsorbed to silver. The Ag(111) surface was modeled using a two-layer 166-atom cluster, with 91/75 atoms in the top/bottom layers, and the coordinates of both layers were kept fixed to match the experimental bulk lattice constant for silver, 4.0862 Å, during the structural relaxations. The ADF calculations were carried out with the DFT-D3 functional [19] built on the revPBE generalized gradient density functional [20–23]. The basis functions on all of the atoms consisted of a triple- ζ Slater-type basis set with polarization functions (TZP) from the ADF basis-set library. The core shells up to 4p for Ag and 1s for C, N, and O were kept frozen. The basis set superposition error (BSSE) was obtained using the Counterpoise method, and in the text we provide the BSSE-corrected binding energies. A fragment orbital analysis [17] was performed on the 3-HPLN/Ag-cluster model using the undistorted metal surface and the molecule (in the geometry of the optimized metal-adsorbate system) as fragments. This yielded the composition of the molecular orbitals (MOs) in terms of the occupied and unoccupied MOs of the fragments.

The most stable 2-dimensional configurations of clusters composed of three 3-HPLN molecules were found using RANDOMDOCK, an automated

stochastic docking program written as an extension to the Avogadro molecular editor [24], which is freely available under the Gnu Public License (GPL) as part of the XtalOpt source code [25]. RANDOMDOCK has been successfully employed to predict the most stable structures of molecularly imprinted polymers and xerogels [26]. Furthermore, an implementation for 2-dimensional systems has been used to locate the global minima of 4-fluorostyrene trimers and tetramers in a study concerning clusters of “magic” sizes which are formed on the Cu(111) and Au(111) surfaces [8]. RANDOMDOCK generates random starting geometries (subject to user defined interatomic distance constraints), which are optimized by an external first-principles program. We used the molecular ADF program for the structural relaxations. For the purposes of this study, the randomly generated configurations were constrained so that all of the molecules lay in the same plane, and the option to force intermolecular hydrogen bonds was employed. Since there are two 3-HPLN conformers from which the trimers can be built, searches were run with 3:0, 2:1, 1:2 and 3:0 ratios of monomer A to monomer B (see Fig. 3(a)), and in total ~2000 geometries were optimized. The 3-HPLN trimers which are lowest in energy were employed to construct structure models which reproduced the main features of the extended networks observed experimentally.

Periodic DFT calculations were performed to model the extended 3-HPLN networks (geometry optimizations, electronic densities of states, charge densities) via the Vienna ab-initio Simulation Package (VASP) version 5.2.11 [27]. The projector augmented wave (PAW) method [28] was used to treat the core states along with a plane-wave energy cutoff of 500 eV. The C/N/O 2s/2p, H 1s and Ag 5s/4p electrons were treated explicitly as valence in the computations. Two functionals which account for dispersion were adopted as described in the text: the DFT-D2 functional [29] was employed to initially (pre)-optimize every system, and the vdW-DF2 [30] non-local correlation functional was used for subsequent optimizations of some systems. Unless otherwise stated, the results presented in the main text were obtained with DFT-D2. The Γ -centered Monkhorst-Pack scheme was used to generate k -point grids of $3 \times 3 \times 1$ and $5 \times 5 \times 1$ for the honeycomb and close-packed (CP) networks of 3-HPLN, respectively. The geometries were converged such that the magnitude of the largest force acting on the optimized atoms was less than 0.02 eV/Å, and the surface was simulated using a two layer slab. A ~20 Å vacuum separated the slab's images along the lattice vector which is perpendicular to the surface. The two layers were fixed at the experimental bulk lattice constant for silver, 4.0862 Å, during the geometry optimizations. A dipole correction was applied along the direction perpendicular to the metal surface using the LDIPOL tag as implemented in VASP.

4. Results and discussion

4.1. Experimental results

When deposited onto Ag(111) at room temperature, 3-HPLN coalesces into short chains that are two molecules across, similar to the chain-like arrangements observed in the bulk 3-HPLN crystal structure [12,31]. The zipper-like chains attract each other on the surface to form small clusters, as shown in Fig. 1(a). Due to the short length of the chains, of just a few nanometer (nm), there exists a high level of disorder in the networks. The chains orient themselves along the $\langle 1\bar{1}0 \rangle$ directions of the surface. We hypothesize that they are H-bonded, with each molecule forming a single H-bond to two different molecules along the chain length as illustrated in Fig. 1(b), reminiscent of the bulk crystal. The chains must attract each other through van der Waals interactions since, within the model, the chemically active hydroxyl and carbonyl groups are participating in hydrogen bonding along the chains. Calculations performed with the DFT-D2 functional, discussed below, suggest that in clusters and networks of 3-HPLN, the intermolecular hydrogen bonding interactions are about an order of magnitude larger than dispersion.

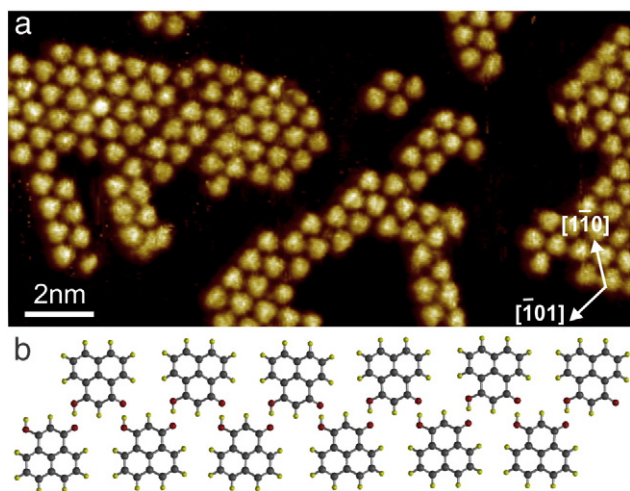


Fig. 1. (a) STM image after room temperature deposition of 3-HPLN on Ag(111). Tunneling parameters: 1 V, 400 pA. (b) Structure model of a hydrogen bonded 3-HPLN chain.

Annealing the sample to approximately 100 °C drastically changes the structure of 3-HPLN on Ag(111), with the emergence of a new ordered network. Fig. 2(a) shows the co-existence of a close packed phase, around the edges of the image, with an ordered porous network in the center. We note that in addition to the trimer based network, when utilizing the same sample preparation procedures we also observe different ordered phases, including one with a dimer comprising the unit cell. This shows that several structural configurations of similar energy coexist, as can also be seen in Fig. 2(a), however only the chiral phase is discussed in this article. The basic building block of the ordered network shown in the STM image is a trimer of 3-HPLN. Two trimers within a rhombus represent the unit cell of the extended network, as highlighted in Fig. 2(c, d). In Section 4.2 we will provide

evidence from first-principles calculations that this trimer configuration is indeed the global minimum structure for three 3-HPLN molecules constrained to 2-dimensions. Each 3-HPLN within the trimer has a single H-bond with each of its two nearest neighbors. Since each carbonyl and hydroxyl group participates in a hydrogen bond within the trimer, there are no carbonyl/hydroxyl groups left to form hydrogen bonds between trimers. It is therefore reasonable to presume that these networks must be held together by van der Waals forces only, similar to the chain-like room temperature phase.

It is clear from the STM images that the trimer networks are porous. In some cases, 3-HPLN molecules were observed within the pores. We believe these to be kinetically hindered 3-HPLN molecules, or a lattice imperfection. Fig. 2(d) shows a schematic of a 3-HPLN trimer coming together to link with an adjacent trimer via the presumably weak van der Waals interactions. From these dimers of trimers, models of left-handed (L) and right-handed (R) extended chiral networks in the STM images in (b) and (c) were constructed, and are also shown in Fig. 2. The van der Waals attraction between adjacent trimers in the porous lattice works as an effective lock and key mechanism, giving the islands long range order.

The structure of the C_{3h} -symmetry 3-HPLN trimer is reduced to C_3 symmetry upon adsorption to the Ag(111) surface (neglecting the atomic arrangement of the underlying surface atoms). As shown in Fig. 2(d), this allows a “handedness” (left or right) to be defined for the cluster, depending on whether the direction of the O–H···O hydrogen bonding contacts point in a counterclockwise direction around the trimer's center of mass (like in the top of Fig. 2(d)) or in a clockwise direction (bottom of Fig. 2(d)). The lack of a mirror plane or glide plane of symmetry perpendicular to the surface gives the adsorbed 3-HPLN trimer local surface chirality at the point group level. Importantly, it is noted that while each pair of 3-HPLN trimers in Fig. 2(d) is shown with only one type of trimer, i.e. each trimer within the pair has the same handedness, there is no reason why this must be the case (unless the mechanism by which they form induces it).

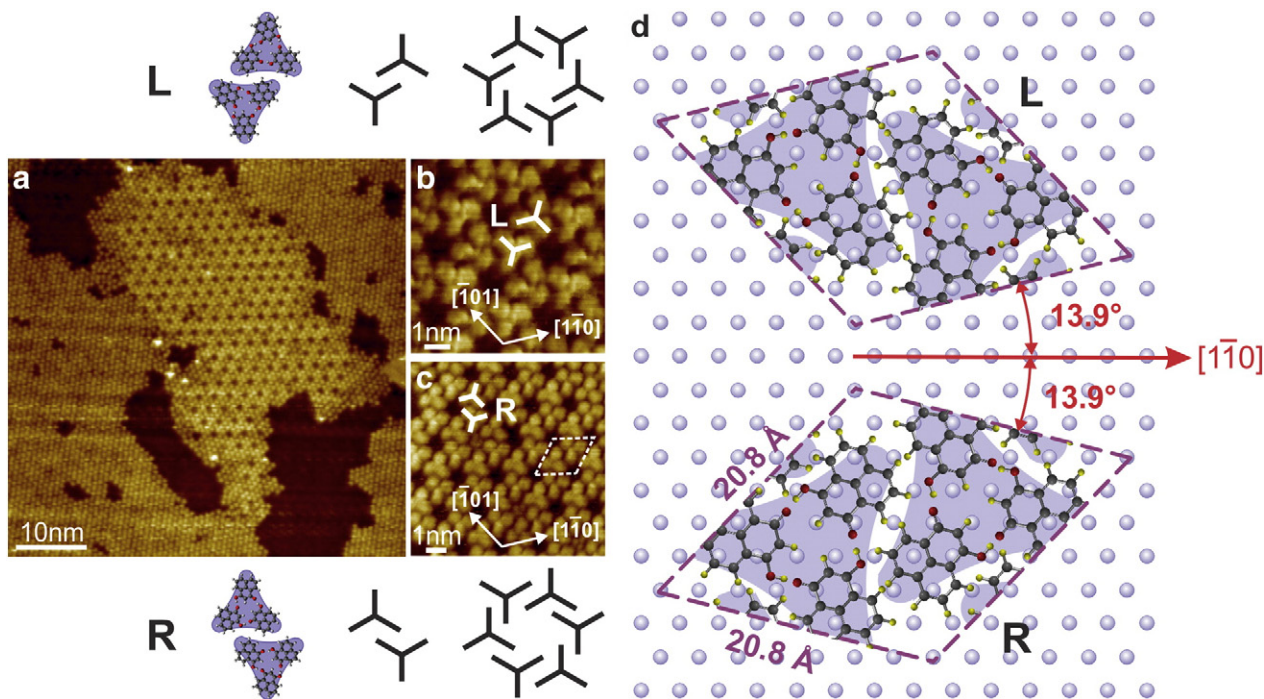


Fig. 2. Networks of 3-HPLN on Ag(111) after annealing the sample to 400 K, followed by cooling to 77 K for STM imaging. (a) STM image highlighting the coexistence of a close packed phase and trimer network phase of 3-HPLN on Ag(111). (b, c) Examples of STM images of left and right-handed networks (enantiomorphs). The structural unit cell is highlighted by dashed lines in (c). Tunneling parameters: (a) -0.2 V, 600 pA; (b) + 0.2 V, 600 pA; (c) -0.2 V, 500 pA. (d) Bonding schematic of two trimers in a unit cell and how this leads to L (left-handed) and R (right-handed) chirality. The epitaxial orientation of the unit cell to the substrate is described as $(2\sqrt{13} \times 2\sqrt{13})13.9^\circ$ in Woods notation. Also shown is how dimers of trimers assemble to form handed porous networks.

The STM images do not reveal the handedness of individual molecules or trimers, but it is reasonable to assume, for now, that each chiral network can be made up of a random mixture of right and left-handed trimers, giving rise to an overall racemic mixture. However, the asymmetric (tilted) packing of the trimers with respect to the diagonals of the unit cell ensures that the extended model networks exhibit surface chirality at the space group level, regardless of the underlying molecular orientation.

The extended network resembles others reported in the literature, for example those formed from melamine on Au(111) [32,33], titanium phthalocyanine (TiOPc) on Ag(111) [34], perylene tetra-carboxylic diimide (PTCDI), melamine on a silver-terminated silicon surface, or self-assemblies of SubPc on Au(111) [11,35,36–38]. What is further striking here is that the epitaxial orientation of the porous 3-HPLN network adsorbed to Ag(111), described as $(2\sqrt{13} \times 2\sqrt{13})R13.9^\circ$, is identical to the epitaxial orientation of TiOPc on Ag(111). Considering the differences between 3-HPLN and TiOPc, namely their chemical constituents and intramolecular bonding, symmetries, and different attachments to the surface, we believe this epitaxial fit to be, at least in part, a coincidence. But, an interesting point to take away from the similarities between the two networks is that two qualitatively similar STM images can be obtained from completely different molecules, even molecular clusters, with different types of intermolecular bonding. This suggests that there might be a common principle guiding the chirality and porosity of networks comprised of very different building blocks. Several of the porous networks reported in the literature are mentioned alongside ones which are close-packed. For example, the energy of a porous network of melamine on Au(111) was lower than that of a close-packed alternative, since the strength of the hydrogen bonding interaction was maximized within it. [32]. In the penultimate section of this article we employ DFT calculations to investigate the relationship between porous networks and plausible close-packed networks, in the context of 3-HPLN.

4.2. Computational results

4.2.1. Monomers and trimers of 3-HPLN

To help set the stage for the discussion of the extended networks of 3-HPLN, we first consider the structure and electronic structure of a single 3-HPLN monomer in the gas phase, and its interaction with the

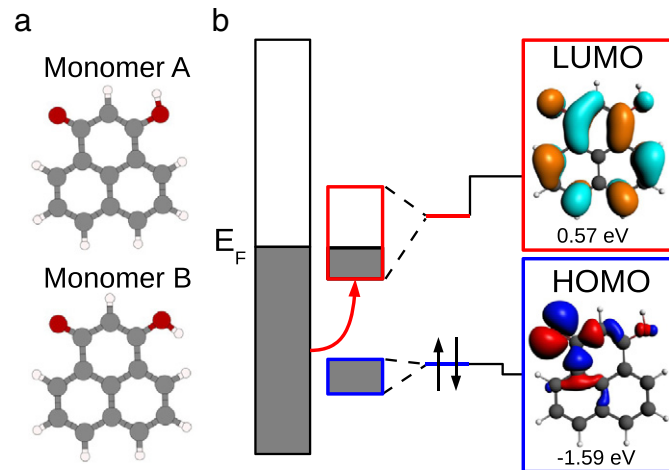


Fig. 3. (a) Two conformers of 3-HPLN which differ by the rotation of the hydroxyl group. (b) A schematic interaction diagram between M_A of 3-HPLN with a 166-atom Ag(111) finite cluster. The panels to the right illustrate the HOMO and the LUMO, isovalue = ± 0.03 au. The red/blue rectangles denote the relative width of the bands resulting from the hybridization between the LUMO/HOMO of the adsorbate with the metal surface MOs. The energies of the MOs have been adjusted such that the HOMO of the 3-HPLN/silver system (Fermi level) is set to 0 eV.

Ag(111) surface. Further, we look closely at a number of low-energy trimers of 3-HPLN in the gas phase and study how their relative energies change upon surface adsorption.

The 3-HPLN molecule has two distinct conformers, monomer A (M_A) and monomer B (M_B) as illustrated in Fig. 3(a), which are related by a 180° rotation of the hydroxyl group. In the gas phase M_A is 0.11 eV/molecule lower in energy. Molecular calculations using a finite cluster model, as described in Section 3, show that on an Ag(111) cluster the relative energy difference decreases to 0.09 eV/molecule. Even though this value is small, it is still 3.5 times larger than kT at room-temperature. The BSSE corrected binding energy of M_A to the Ag(111) cluster model, 2.04 eV/molecule, is comparable to other systems we have studied, such as a quinonoid zwitterion adsorbed to Ag(111) [39].

In Fig. 3(b) we provide a schematic diagram showing the interactions between the highest occupied and lowest unoccupied molecular orbitals (HOMO and LUMO) of the most stable conformer of 3-HPLN and the MOs of the silver surface model. We have found this approach useful in analyzing the bonding between the substrate and adsorbate, and thinking about how it may influence the supramolecular interactions between the adsorbed molecules [8,39,40,41]. The 3-HPLN LUMO, which has π -symmetry with respect to the plane of the molecule but has σ -overlap with s and select d orbitals of the metal surface, broadens significantly upon adsorption and has non-negligible contributions to states throughout a wide energy range which span above and below the Fermi level (in our finite model this corresponds to the HOMO of the total system). This interaction leads to the partial population of the LUMO of 3-HPLN, and therefore to a transfer of charge from the surface to the molecule. A Hirschfeld analysis shows that the charges on M_A and M_B are comparable, and we estimate them to be $-0.26e$ and $-0.29e$, respectively. The HOMO of 3-HPLN has σ -symmetry with respect to the plane of the molecule, and is therefore more localized to this plane than the LUMO. As a result, the spatial overlap of the metal orbitals is smaller with the HOMO than with the LUMO, so the HOMO/surface states are less disperse. The alignment of the organic's LUMO with the Fermi level of the metal, and the concomitant charge transfer from the silver surface to the adsorbate, has been noted in a number of studies of small-to-large organic molecules adsorbed onto metallic surfaces [42]. Moreover, it is supported by the electronic structure of the periodic networks described later in the text.

A stochastic docking program was employed to search for the lowest energy trimers composed of varying ratios of the two monomers of 3-HPLN. The relative energies of the most stable trimers we found, illustrated in Fig. 4, are given in Table 1. The order of stability is not surprising, and it correlates with the number of intramolecular hydrogen bonds, and with the ratio of the two monomers comprising the trimer. In the gas phase, the lowest energy trimer, trimer A or T_A , is composed of three molecules of M_A which are hydrogen bonded to each other such that each molecule donates one and accepts one hydrogen bond, as shown in Fig. 4(a). This cluster has C_{3h} -symmetry and it fully matches the structure model derived from the STM image in Fig. 2. The other trimers we found are composed of different ratios of the two monomers, have C_s -symmetry, and are illustrated in Fig. 4(b, c, d).

When adsorbed to a two-layer surface slab the relative energies between the trimers remained relatively unperturbed, as shown in Table 1. The most notable change is in how the DFT-D2 functional lowers the already small difference in energy between T_A and T_B . The geometry optimization of T_D with the DFT-D2 functional did not converge, however this trimer was computed to be nearly half an eV higher in energy than T_A in the gas phase and on the surface with the vdW-DF2 functional. Moreover, since two-dimensional tilings built from this trimer are not compact enough to resemble the networks observed experimentally, we did not consider it further. Surface adsorption decreases the symmetry of the clusters such that if we neglect the orientations of the molecules with respect to the surface atoms

the point group of T_A becomes C_3 , whereas the other trimers adopt C_1 -symmetry. Thus, all of these trimers exhibit surface chirality at the point group level.

4.2.2. Chirality in extended networks of 3-HPLN

The trimers shown in Fig. 4(a, b, c) can be used to build networks which possess the main structural features of the STM images illustrated in Fig. 2, see for example the tilings constructed from T_A (hcA), T_B (hcB) and T_C (hcC), which are shown in Fig. 5(a). The simulation cells for each honeycomb were made by placing two 3-HPLN trimers of the same handedness in a hexagonal cell such that the center of mass of each trimer, marked by a spiral in Fig. 5(a), lies roughly along the long diagonal of the cell. This construction leaves the region near the cell vertices devoid of 3-HPLN, thereby replicating the pores present in the STM images. The length of the lattice vector corresponds to the distance between the center of one pore to the center of its nearest-neighbor. The pores and the asymmetric packing of the 3-HPLN trimers give rise to the chirality of the networks at the space group level, as described below.

Let us first consider the hcA honeycomb; the location of its symmetry elements are schematically highlighted in Fig. 6. In this hypothetical network each 3-HPLN trimer, represented by the skewed triangles, possesses the same handedness. If we neglect the position of the underlying surface atoms there is a C_3 rotational axis in the center of the trimer motifs, and a C_6 rotational axis in the center of the pores. The $p6$ wallpaper group describes this extended 2-dimensional network, which is therefore chiral. As shown in the Supplementary information, SI, the networks derived from hcB and hcC are chiral too, belonging to the $p2$ wallpaper group. We also considered a tiling constructed from a unit cell comprised of two T_A enantiomers, illustrated in Fig. 5(b). The pattern it gives rise to is also chiral, with $p3$ -symmetry. The chirality of all of these networks arises from the aforementioned asymmetric packing that the trimers have around the pores, and the tilt which they have with respect to their neighbors, which prohibits any mirror planes of symmetry perpendicular to the plane of the surface. As a result, the chirality will be maintained no matter how the handedness of the underlying trimers is assigned.

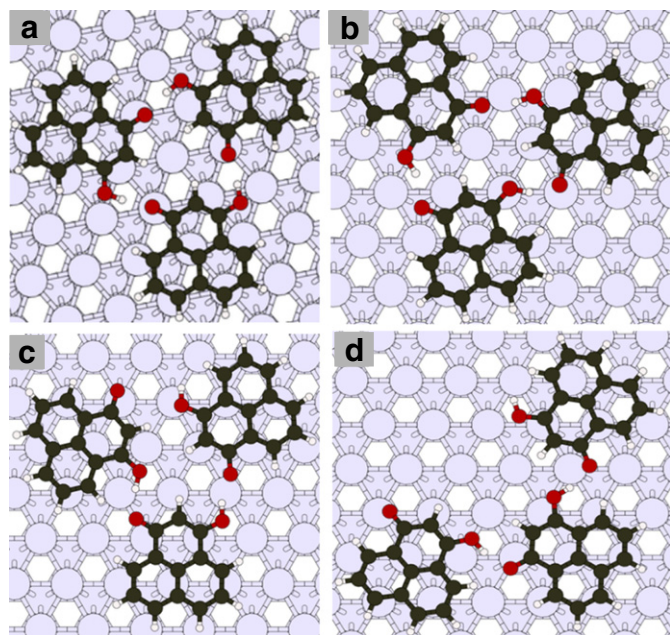


Fig. 4. 3-HPLN trimers lowest in energy that were found for a (a) 3:0 (T_A), (b) 2:1 (T_B), (c) 1:2 (T_C) and (d) 0:3 (T_D) ratio of M_A to M_B . All of the trimers are shown in their optimized geometries over a two layer Ag(111) slab.

Table 1

Relative energies (eV/molecule) of the trimers illustrated in Fig. 4. The computations were carried out with VASP using the vdW-DF2 functional in the gas phase ($\Delta E_{\text{gas}}^{\text{vdW} - \text{DF2}}$), and adsorbed on the Ag(111) surface ($\Delta E_{\text{surf}}^{\text{vdW} - \text{DF2}}$). The relative energies on the surface computed using the DFT-D2 functional ($\Delta E_{\text{surf}}^{\text{DFT} - \text{D2}}$) are also shown.

Trimer	$\Delta E_{\text{gas}}^{\text{vdW} - \text{DF2}}$	$\Delta E_{\text{surf}}^{\text{vdW} - \text{DF2}}$	$\Delta E_{\text{surf}}^{\text{DFT} - \text{D2}}$
T_A	0.00	0.00	0.00
T_B	0.16	0.23	0.08
T_C	0.39	0.36	0.43
T_D	0.50	0.46	–

4.2.3. The honeycomb networks in the gas phase

Periodic planewave DFT calculations were carried out to study these networks first in the gas phase, and subsequently on an Ag(111) surface. Unless otherwise stated, the dispersion corrected DFT-D2 functional was employed in what is presented below. Preliminary computations were performed to determine the relative energies of the hcA, hcB and hcC honeycombs in the gas phase. The networks were simulated using a hexagonal cell with 25 Å spacing between the voids, because it was found that in the gas phase hcA buckles within smaller simulation cells when optimized using the PBE functional. At this spacing the computed relative energies of hcA/hcB/hcC are 0/0.06/0.25 eV/molecule within DFT-D2 and 0/0.08/0.26 eV/molecule within PBE. The similarity of the relative energies computed with and without the post-SCF dispersion corrections implies that the van der Waals interactions in the three honeycombs are quite uniform. Moreover, the relative energies of the networks correlate with those of the isolated trimers from which they are built, suggesting that the stability of the extended system arises from the number of hydrogen bonds between the trimers and the ratio of M_A to M_B within them.

We further considered a network similar to hcA, but it was composed of one left-handed T_A trimer and one which was right-handed, as illustrated in Fig. 5(b). The energy difference between this tiling and hcA was quite small, less than 0.01 eV/molecule. When these two honeycombs were optimized with lattice vectors measuring 23, 24, and 26 Å instead, the difference in energy was always found to be less than 0.02 eV/molecule. This suggests that, in these models, the trimeric clusters within a single unit cell are also held together via weak dispersion interactions whose strength does not depend upon the handedness of the trimeric building blocks. Our calculations show that a racemic mixture of T_A is effectively isoenergetic with a network comprised of a single chirality at these coverages. Therefore, entropy will likely favor the formation a racemic mixture of T_A , since there are many ways in which the trimers can be arranged vs. a mixture which is enantiomerically pure. At slightly higher coverages, with 22 Å lattice vectors, the networks which are constrained to be planar do show a much wider spread in energy of 0.14 eV/molecule, suggesting that the network is becoming sensitive to the subtle differences in shape when one enantiomer is substituted for another. At this coverage in the gas phase the non-planar networks are >0.55 eV/molecule more stable than the planar ones. At coverages corresponding to those observed in experiment the networks optimized on the surface (see below) buckle. Further studies are necessary to determine exactly how the handedness of the building blocks affects the energy of the more densely packed, buckled networks.

4.2.4. The honeycomb networks on the Ag(111) surface

Since the hcA network was found to be the lowest in energy in the gas phase, and is consistent with the structure model proposed from experiment, we considered its interaction with the Ag(111) surface. First, its geometry was optimized over a simulation cell with 26.0 Å lattice vectors, corresponding to a 162-atom 9×9 supercell of a primitive hexagonal Ag(111) unit cell which is two-layers deep. The binding energy of hcA, defined as the energy of the total optimized system subtracted from the sum of the energies of the isolated slab and an

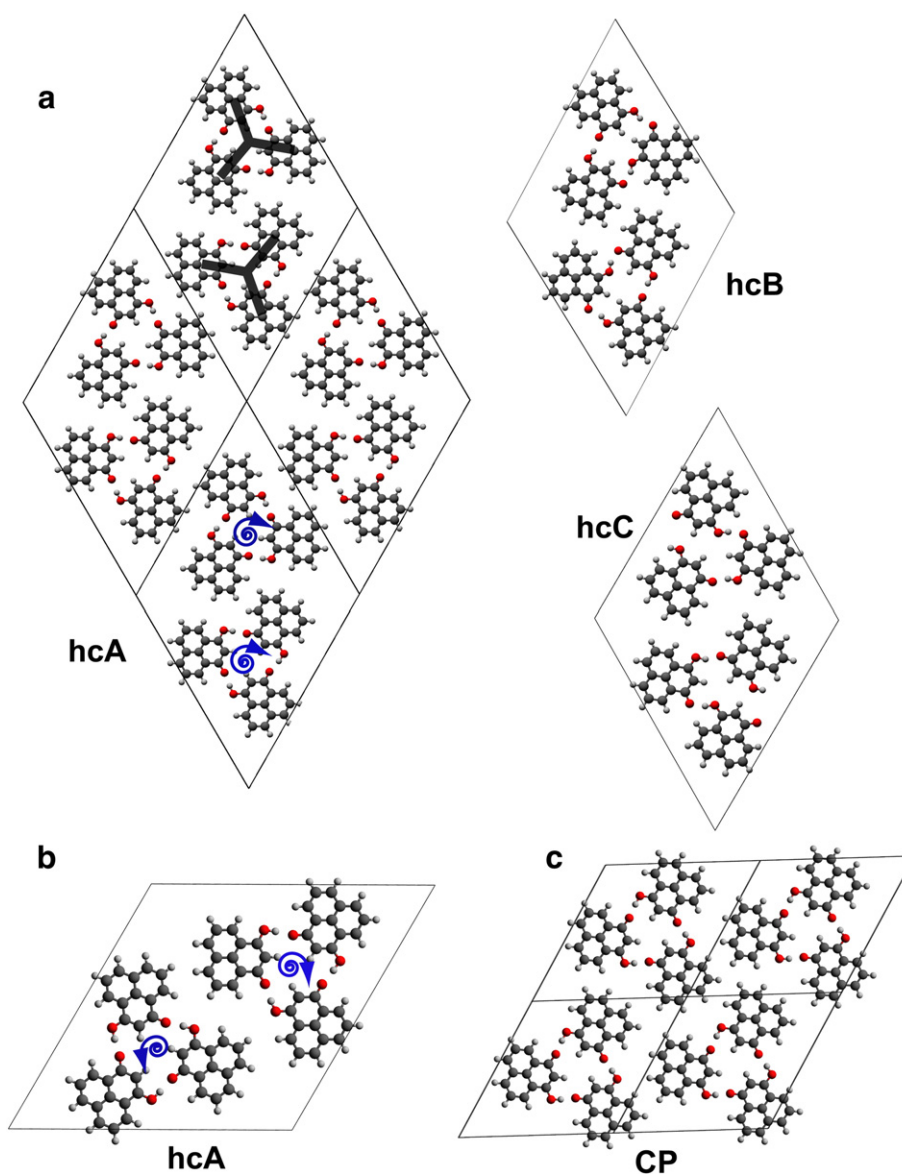


Fig. 5. (a) Simulation cells of the hcA, hcB, and hcC honeycombs, which are constructed from the T_A , T_B and T_C trimers of 3-HPLN, respectively, see Fig. 4. A supercell of hcA is shown to illustrate the pores in the lattice more clearly. The blue spirals are placed at the center of mass of the trimers, and indicate their handedness. (b) A variation of the hcA model which is constructed from two T_A trimers with opposite handedness. (c) A hypothetical close-packed (CP) model structure of 3-HPLN.

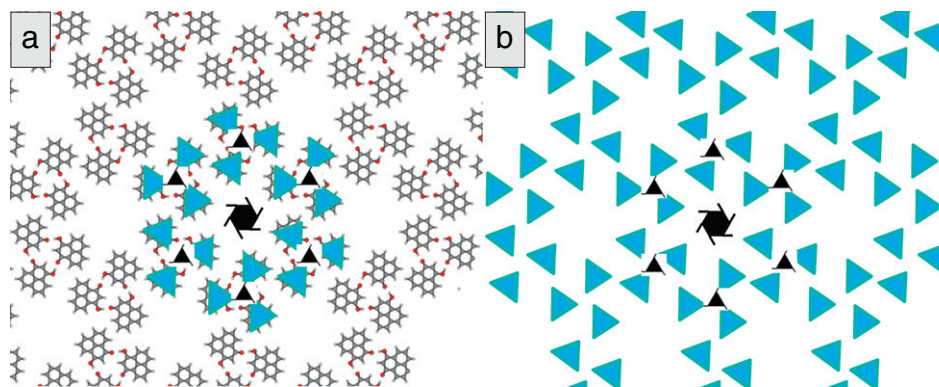


Fig. 6. (a) An extended honeycomb network composed of T_A trimers with the same handedness, along with an overlay of a schematic which represents each 3-HPLN molecule by a blue triangle. (b) The same network as in (a) further simplified. The black triangles within the trimers, and the hexagon at the center of the pore illustrate the C_3 and C_6 rotation axes and their handedness. The Ag(111) surface has been omitted for clarity.

ensemble of non-interacting 3-HPLN molecules [$BE = (E_{\text{Ag}(111)} + \sum_i^n E_{3\text{-HPLN}} - E_{\text{hcA}/(\text{Ag}111)})/n$] was computed to be 2.33 eV/molecule. The binding energy can be further decomposed into a term which accounts for the interaction of the 3-HPLN molecules within a gas phase hcA network (whose geometry corresponds to the one adopted on the surface), and the adsorption of this network to the surface. We compute these values to be 0.64 and 1.69 eV/molecule, respectively, suggesting that the substrate–adsorbate interactions account for nearly three quarters of the total binding energy.

The interaction energy of the 3-HPLN molecules within the optimal adsorbed hcA network in the gas phase, 0.64 eV/molecule, can further be decomposed into terms which describe the binding strength of 3-HPLN molecules coming together to form trimers (0.60 eV/molecule), the dispersion interactions between the trimers (0.04 eV/molecule), and the amount of energy required to distort the geometry from the nearest local minimum on the gas-phase potential energy surface to that which is found on the substrate (−0.02 eV/molecule). Unsurprisingly, the binding within the 3-HPLN trimer, which includes hydrogen bonding, is an order of magnitude larger than the dispersion interactions between trimers, and the geometrical distortion destabilizes the network only slightly. In order to study the effect of the slab on the dispersion interactions between the trimers, we considered the addition of a single T_A within the unit cell of hcA to an Ag(111) surface upon which the second trimer was already adsorbed in the optimized geometry of the total system. The calculated binding energy, 1.73 eV/molecule, was only ~0.04 eV/molecule stronger than the binding energy of the entire 3-HPLN network, which matches the ~0.04 eV/molecule interaction energy between trimers in the absence of the surface. This illustrates that, at this level of theory, the slab has virtually no effect on the dispersion interactions between the trimers at this coverage.

The reorganization of electronic charge that occurs between the substrate and the adsorbate was analyzed by calculating the difference between the charge density of the total system and that of the isolated fragments; the fragments are: 1) the Ag(111) slab, and 2) the gas-phase hcA network in the geometry it assumes on the surface. We further scrutinized how the electron density difference compares when the fragments are: 1) the silver slab with one of the two T_A trimers in the unit cell already adsorbed, and 2) the second trimer in the gas phase. The charge reorganization was found to be qualitatively similar in the two calculations, but the latter also shows how the two trimers influence each other's electron density and its computed charge density difference, $\Delta\rho_{\text{diff}}$, is illustrated in Fig. 7. The isosurface of $\Delta\rho_{\text{diff}}$ which is shown is supplemented by contour plots of $\Delta\rho_{\text{diff}}$ within two planes at different heights and parallel to the surface, these planes help illustrate the topology more clearly. The blue regions denote a depletion of the electron density, relative to the fragments, and are most evident below the molecule (top panel), and just above the surface (bottom panel). The red regions illustrate a slight accumulation of charge near the surface surrounding the molecule. This charge redistribution is consistent with the so-called 'pillow effect' [43], which dictates that the electron density just below the molecules and just above the surface decreases upon adsorption as a result of Pauli repulsion. The regions between the two planes shown in Fig. 7 are more complex.

The schematic level diagram obtained by analyzing our molecular calculations in Fig. 3(b) indicates that charge is transferred from the silver surface to the LUMO of 3-HPLN upon adsorption. The LUMO has substantial C–C p - π bonding character across the carbons comprising the ring to which the carbonyl and hydroxyl groups are bound. In full agreement with this analysis, the two-dimensional slice of $\Delta\rho_{\text{diff}}$ just below the plane of the molecule shows regions of charge accumulation (red regions) in the π system of the circled C–C bonds. The 3-HPLN site-projected densities of states (PDOS) shown in Fig. 7(b) also agree with the results obtained from the molecular calculations. The green line denotes C and O p -character which is perpendicular to the plane of the molecule, whereas the red, blue, and black lines are representative

of character arising from H, C and O s -orbitals and the p -orbitals within the plane of the molecule, i.e. the σ -system. The LUMO of 3-HPLN lies just above the Fermi level, but upon adsorption it broadens significantly and crosses the Fermi level such that there is a transfer of charge from the surface to the molecule. The HOMO is less disperse and is found at ~2.2 eV below the Fermi level. The HOMO-1 and HOMO-2 are of C and O π -character and their energies are within 0.5 eV of the HOMO in the gas phase. The p_z character which is found between −1.5 and −4.5 eV is likely due to these, and other occupied orbitals which are primarily of π -symmetry with respect to the molecular plane.

The 26.0 Å inter-pore separation used thus far in the calculations is much larger than the distance of 20.8 Å estimated from the STM images. Therefore, the hcA structure was further optimized over a two-layer Ag(111) slab with ~23.1 Å lattice vectors, commensurate with an 8×8 supercell of the primitive hexagonal Ag(111) cell, which is two layers deep and has a coverage of 1.30 molecules/nm². The binding energy of hcA to the silver surface computed with this structure model is 2.31 eV/molecule, which is in good agreement with the 2.33 eV/molecule calculated within the larger simulation cell. The calculated charge density difference plot (see Fig. 7(c)), and total DOS/PDOS plots (see the SI) also matched well with the expanded lattice. We note that at this spacing the network buckles slightly, and the trimers tilt somewhat. This leads to a larger energy difference between the geometry adopted on the surface and the optimal gas-phase geometry, becoming −0.09 eV/molecule.

Finally, the binding energy of the hcA network constrained to the simulation cell identified from the experiment, with 20.8 Å lattice vectors and a coverage of 1.60 molecules/nm², was computed to be 1.93 eV/molecule. The drop in binding energy with respect to the 1.30 molecules/nm² network (1.93 eV/molecule vs. 2.29 eV/molecule) correlates mostly with the weaker interaction the network has, as a whole, with the surface (1.33 eV/molecule vs. 1.69 eV/molecule). This weaker interaction, in turn, stems from the buckled 3D structure of the 3-HPLN network, wherein one of the two 3-HPLN trimers in the simulation cell bends away from the surface to form a propeller-like shape. The binding energy of 3-HPLN molecules to create the trimers also decreases to 0.48 eV/molecule (from 0.62 eV/molecule at a coverage of 1.30 molecules/nm²). When computed with respect to the coverage, instead of the number of adsorbed molecules, the binding energy of the 1.60 molecules/nm² network is lower than that of the 1.30 molecules/nm² network, −3.07 eV/nm² vs. −2.96 eV/nm². This is because the density of molecules is greater at the higher coverage (even though each molecule interacts with the surface less strongly).

4.2.5. An alternative close packed network

In the honeycomb networks constructed from T_A , each 3-HPLN molecule is surrounded by five other molecules; the two molecules which belong to the same trimer are connected via hydrogen bonds, and the other three interact via van der Waals forces. If dispersion between the trimers was the only factor important in determining the way in which they self-assemble, one would expect that a close-packed (CP) configuration where each 3-HPLN interacts with four nearby molecules via dispersion would be favored instead. One example of such a CP tiling is illustrated in Fig. 5(c), whose unit cell contains a single T_A . The resulting network is comprised of trimers with a single handedness, and it is chiral with the $p3$ wallpaper group. Unlike the honeycomb structures, however, it is possible to construct 2-dimensional CP networks which are globally achiral by using mixed left- and right-handed trimer building blocks. We also note that, due to the weak van der Waals attractions between trimers and the rather unspecific binding between the 3-HPLN molecules and the surface, a number of other network architectures (some chiral, others not) are possible. For example, a non-hexagonal close-packed network with the same number of offset trimer–trimer interactions per molecule as hcA, three, was discussed for melamine on Au(111) surfaces [32]. In this work, we consider only the CP network in Fig. 5(c) as an example

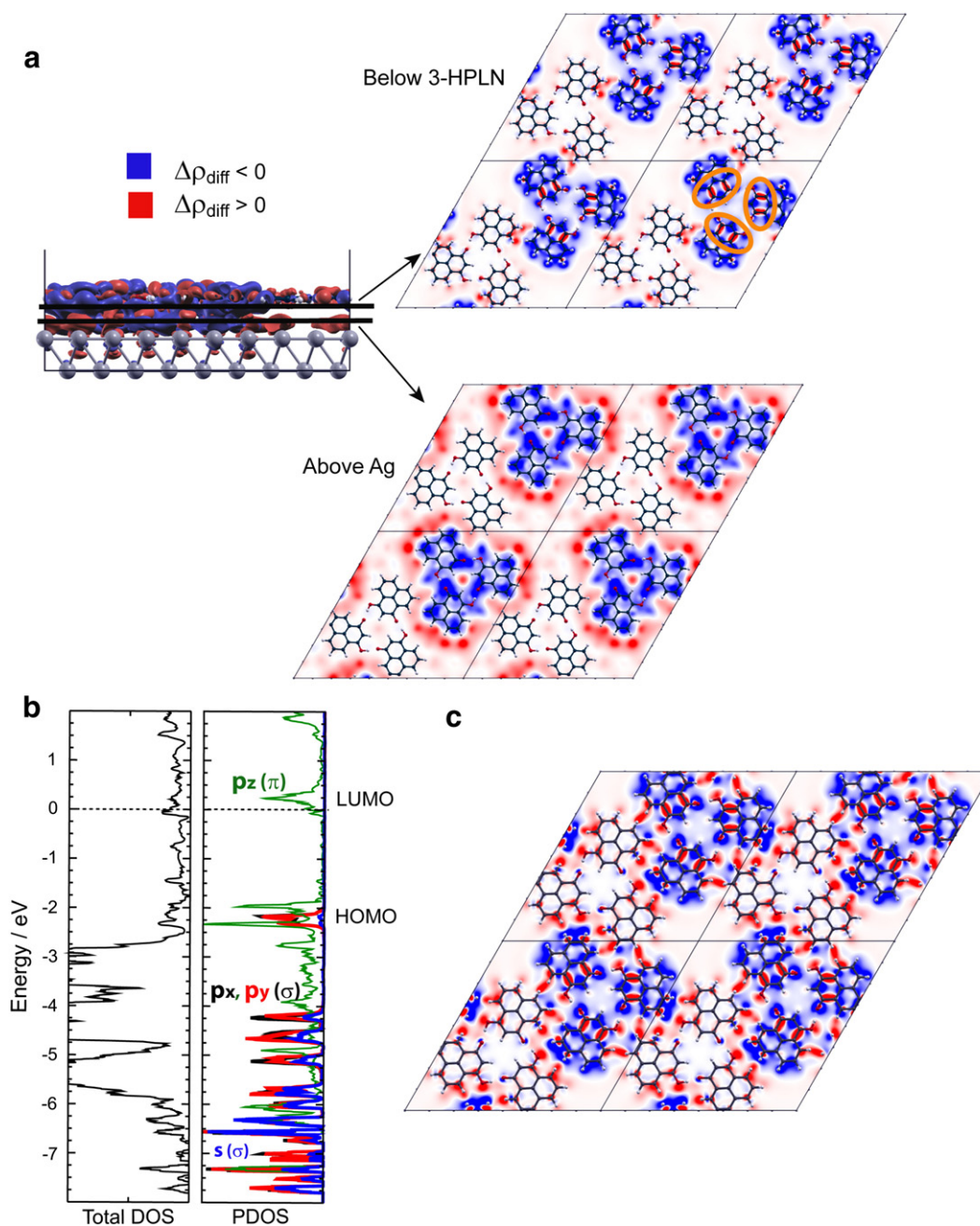


Fig. 7. (a) The charge density difference, $\Delta\rho_{\text{diff}} = \rho(\text{hcA}/\text{Ag}(111)) - \rho(T_{A1}/\text{Ag}(111)) - \rho(T_{A2})$, computed using a unit cell with lattice vectors measuring 26.0 Å. It illustrates the charge reorganization which occurs when the second trimer in the unit cell, T_{A2} , adsorbs to an Ag(111) lattice which already contains one such trimer, T_{A1} . (b) Total density of states of hcA on an Ag(111) slab with lattice vectors measuring 26 Å, and the summed site-projected densities of states of the H, C and O, s , p_x , p_y and p_z orbitals. The z -direction is perpendicular to the plane of the surface. (c) Same as (a) but for a system whose lattice vectors measure 23.1 Å, the plane is chosen to lie just below the 3-HPLN molecules.

of a close-packed network which may be competitive with hcA, in the hopes of determining the reason why it, and related systems, are not observed in experiment. It should also be pointed out that the close packed phase in Fig. 2(a), outside the porous network, is not made up of trimers of 3-HPLN, but rather of monomers.

The binding energy of the CP network (with one or two 3-HPLN trimers per cell) was calculated to be 2.33–2.36 eV/molecule using coverages of 1.33 and 1.48 molecules/nm², respectively. These coverages were chosen since their intermolecular 3-HPLN to 3-HPLN distances are comparable to the hcA structure whose lattice vectors measure 23 Å but, because of the pores, the coverage is appreciably higher than in the hcA model (which is 1.30 molecules/nm²). The calculated binding energies are certainly comparable, albeit slightly higher,

than the 2.29–2.33 eV/molecule binding energy obtained for hcA at the lower coverages. The binding energies expressed per unit area of surface are 3.16 eV/nm² (for the 1.33 molecules/nm² coverage) and 3.45 eV/nm² (for the 1.48 molecules/nm² coverage). The PDOS of the 1.33 molecules/nm² CP network agrees well with the one computed for hcA shown in Fig. 5(b), illustrating that the electronic interactions with the Ag(111) surface do not depend much upon the patterns the trimers form. Further calculations were carried out to investigate if the corrugations in the potential energy surface, or a preference of the binding site of 3-HPLN to Ag(111), may be important in determining the network architecture. Several binding sites were sampled for the CP network and the optimized energies were found to differ by roughly 0.03 eV/molecule, suggesting that the potential energy surface is quite

flat. We do note, however, that this energy difference is comparable to the difference in energy between the gas-phase CP and hcA networks, and the strength of the trimer–trimer interactions.

Since we further wanted to see how the binding energy is affected at coverages near 1.60 molecules/nm², a 1.66 molecules/nm² CP network was also considered. The binding energy was found to be 2.08 eV/molecule, or 3.45 eV/nm². Like hcA, the binding energy per molecule decreases at higher coverages, and, also like hcA, the binding energy per unit area of the surface increases from ~1.30 eV/nm² coverage. The two 3-HPLN trimers in the simulation cell of the 1.66 molecules/nm² coverage CP structure also buckle away from the surface, but the biggest difference between them and the 3-HPLN trimers in hcA at 1.60 molecules/nm² is the approximate symmetry. In hcA, the hydrogen-bond distances and the distances between the central carbon atoms on adjacent 3-HPLN molecules within a trimer are fairly consistent, measuring ~1.53 Å/~1.58 Å and 9.04–9.06 Å/8.94–9.00 Å (considering each trimer in the simulation cell separately), respectively. The range of hydrogen bond distances match up surprisingly well with those observed in an isolated 3-HPLN trimer, 1.58–1.59 Å. In CP, the hydrogen-bond distances range from 1.46–1.55 Å/1.49–1.52 Å and the distances between 3-HPLN molecules within each trimer range from 9.02–9.19 Å to 8.92–9.20 Å. Furthermore, the shortest distances between 3-HPLN molecules which belong to different trimers is much smaller in hcA than in CP; for example the average distance of the two shortest 3-HPLN to 3-HPLN contacts is 7.29 Å in hcA vs. 7.80 Å in CP, despite the lower coverage of hcA. This suggests that the neighboring trimers are packed closer together in hcA, and the packing is done in such a way that the strain on each trimer is minimal. The driving force behind the formation of hcA over CP may be related to distortions of the 3-HPLN trimers in CP and, therefore, the weakening of its hydrogen bonds, similar to what was proposed for networks of melamine on Au(111) [32]. However, we note that the constraints of the CP simulation cell used, which contained only two 3-HPLN trimers, ensures that each trimer is in contact with its own mirror image, and it is likely the trimers would relax to a slightly different geometry in an appropriate supercell.

In summary, at coverages close to those observed experimentally, the binding energy of 3-HPLN to the Ag(111) surface to form the CP network is larger than that for hcA. However, the energy differences are small, and are comparable to the strength of the interaction between the 3-HPLN trimers and the corrugations in the potential energy surface. It is highly possible that these energies may be influenced by the level of theory we applied and the slab model, but in light of the small energy differences encountered in this study we wondered whether other factors, typically not considered in explaining the structures which form upon self assembly, could be significant in determining which extended systems – the porous honeycomb networks in which the trimers are offset, as opposed to non-offset unit cells and/or close-packed tilings – are preferred.

A key difference between the two types of networks is that neighboring trimers are closer together in hcA than in CP, suggesting that the “shape” of a 3-HPLN trimer is more suited to hcA. The effective shape that a trimer assumes resembles a rounded triangle. The rounded triangle structural motif features prominently in recent studies of networks of hard Brownian regular (achiral) triangles confined to two dimensions [15]. It was found that at packing fractions greater than 0.61, rotational entropy was crucial in determining the arrangement of neighboring triangles [15]; the role of shape [45] entropy in determining the patterns adopted in two and three dimensions has also been discussed. In Ref. [15] it was argued that the rotation of the triangles about their center of mass gives rise to an effective trioid shape (a rounded triangle which resembles the 3-HPLN trimers), see Fig. 8(b), and that the close packing of such trioids could be employed to explain the spontaneous formation of local chiral domains from equilateral triangles which interact with each other simply by shape exclusion. The argument that rotational entropy can lead to chirality

was disputed by Carmichael and Shell [16], wherein it was shown that the trioid shape by itself can promote chirality, and the degree of particle roundedness can influence the structural motifs.

Regardless of the debate, both Mason's and Shell's studies are intriguing. The 3-HPLN trimers form a trioid shape (whether they are rotated or not), and the unit cell we observe in experiment clearly matches up with the best packing of two such trioids. This is likely why the trimers are closer to each other in hcA than in CP. Similar motifs emerge in Mason's and Shell's work: the “rounded triangles” are offset from each other, but none of their networks match up exactly with the honeycombs seen here. Of course neither Mason's nor Shell's models account for all of the intricate interactions in the 3-HPLN systems, like the van der Waals attraction between trimers and the 3-HPLN/surface interactions. Nonetheless, these studies hint that the rotational entropy or effective shape may indeed be important factors in determining the chirality and porosity of the networks of 3-HPLN on Ag(111). Indeed, it was recently illustrated that entropy can have a dramatic influence on the self-assembly of 1,4-substituted benzenediamine on Au(111) surfaces [44].

It is worth mentioning a few explanations that have been invoked to justify the formation of similar chiral and porous networks. The most notable of these is the case of melamine on Au(111). The self-assembled network was deemed to be a result of a kinetic pathway in which substrate Au atoms act like a catalyst by forming intermediate melamine-Au compounds [33]. This model, however, is likely not applicable here since our triangular-shaped building blocks do not have any attachment points, such as the N atoms of melamine, to which Au atoms from the substrate could bind. The origin of the observed pores in the networks of TiOPc, as seen in Ref. [34], was attributed to local electric dipoles. Likewise, this concept is not easily applicable here, although we do note that dipolar effects due to the charge transfer at the organic–metal interface, particularly with the low-lying 3-HPLN LUMO, and the associated charge screening by the substrate, might certainly be important for the self-assembly.

5. Conclusions

Scanning tunneling microscopy was employed to study the self-assembly of 3-HPLN on the Ag(111) surface. Annealing leads to the formation of a porous honeycomb network whose building blocks are trimers of 3-HPLN molecules aligned in such a way that they are offset with respect to the diagonal of the unit cell. Density functional theory calculations, which incorporate the effects of dispersion, illustrate that the 3-HPLN molecules within the trimer are hydrogen bonded to each other such that each molecule donates one and accepts one hydrogen bond. The trimers interact with each other via dispersion interactions, which are about an order of magnitude weaker than the hydrogen bonds. In two dimensions the 3-HPLN molecules are chiral, as are the trimers they form. Configurational entropy favors the presence of a racemic mixture of trimers on the surface, but computations hint that at high coverage the subtle shape differences of the enantiomers may energetically favor a particular geometric arrangement. Irrespective of the handedness of the trimers comprising the extended structure, the networks are chiral at the space group level because of the asymmetric arrangement the trimers have around the pores.

Interestingly, motifs resembling those observed in our work, which are comprised of rounded triangles, have previously emerged in experiments and simulations probing the way how achiral objects interact with each other via their shape only [15,16]. An offset unit cell is the best way to pack triangles which have been rounded (either as a result of their shape, or because of rotational entropy). We speculate that these factors, typically not considered in surface self-assembly, may be important in determining the networks that form. They represent intriguing design parameters in self-assembly. It should be noted, however, that neither one of these factors alone can fully explain why a porous chiral network is favored over a closed packed one. In fact,

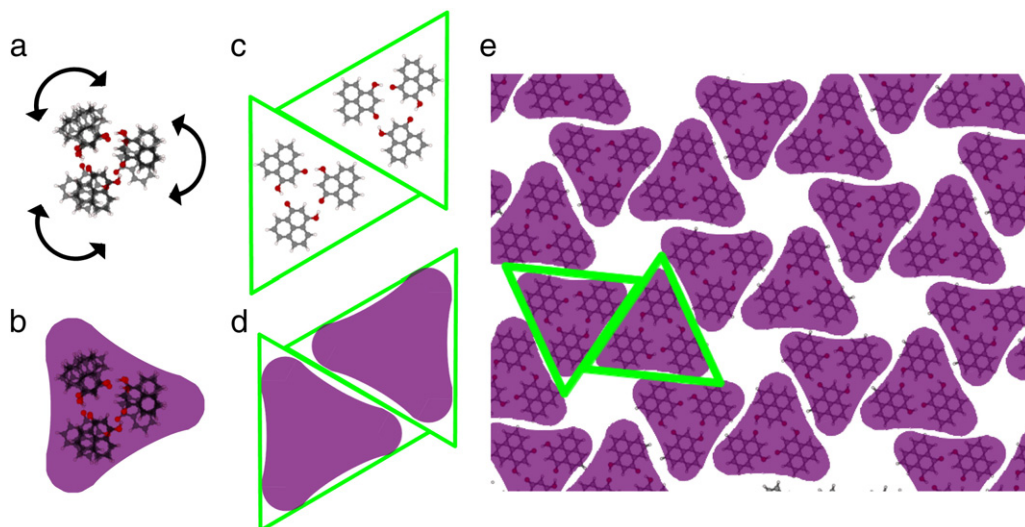


Fig. 8. (a) The rotation of a 3-HPLN trimer gives rise to the (b) trioid shape (purple). This trioid encompasses the area which the trimer traverses upon rotation around its center of mass. Note that the unrotated trimer can also be approximated as a trioid. (c, d) The best packing of two trioids is when they are offset from each other. Such trioids fit well within the unit cell derived from experiment (see Fig. 2(d)). (e) A schematic illustration of the trioids comprising the hcA honeycomb lattice.

neither the binding energy, charge transfer, nor the epitaxy arguments could fully resolve this issue. Other factors that would potentially support network hcA over CP are charge pillow build-up around the adsorbed molecules [41], surface dipole formation due to charge transfer from the substrate to the molecules, and coverage-dependent intermolecular bond strength [46]. Although these effects are incorporated into the electronic-structure computations, it should be stated that the dispersion corrected density functional employed (DFT-D2) is known to overbind, thereby leaving room for future studies.

Acknowledgments

Support from the Center of Computational Research at SUNY Buffalo is acknowledged. The authors thank Zackary Falls for implementing the 2D structure search option in the RANDOMDOCK source code. E.Z. thanks the Alfred P. Sloan Foundation for a Research Fellowship (2013–2015). J.H. acknowledges financial support from the Homing Plus Program (HOMING PLUS/2012-6/4) granted by the Foundation for Polish Science and co-financed by the European Regional Development Fund. A.E. acknowledges funding through NSF MRSEC (DMR-0820521), NSF Grant EPS-1004094 and SRC gift no. 2013-RJ-2365G.

Appendix A. Supplementary data

Optimized coordinates for each system, and select densities of states plots. Schematic illustrations of possible networks, and their symmetry classifications. Supplementary data to this article can be found online at <http://dx.doi.org/10.1016/j.susc.2014.04.015>.

References

- [1] R. Raval, *Chem. Soc. Rev.* 38 (2009) 707.
- [2] K.-H. Ernst, *Phys. Status Solidi B* 249 (2012) 2057.
- [3] M. Ortega Lorenzo, C.J. Baddeley, C. Muryn, R. Raval, *Nature* 404 (2000) 376.
- [4] F. Zaera, *J. Phys. Chem. C* 112 (2008) 16196.
- [5] Y. Izumi, *Adv. Catal.*, 321983. 215.
- [6] Y. Orito, S. Imai, *J. Chem. Soc. Jpn.* 8 (1979) 118.
- [7] S.M. Barlow, R. Raval, *Surf. Sci. Rep.* 50 (2003) 201.
- [8] A. Jewell, S. Simpson, A. Enders, E. Zurek, C. Sykes, *J. Phys. Chem. Lett.* 3 (2012) 2069.
- [9] T.J. Lawton, J. Carrasco, A.E. Baber, A. Michaelides, E.C.H. Sykes, *Phys. Rev. Lett.* 107 (2011) 256101.
- [10] Q. Li, C. Han, S.R. Horton, M. Fuentes-Cabrera, B.G. Sumpter, W. Lu, J. Bernholc, P. Maksymovych, M. Pan, *ACS Nano* 6 (2012) 566.
- [11] W. Xiao, X. Feng, P. Ruffieux, O. Groning, K. Mullen, R. Fasel, *J. Am. Chem. Soc.* 130 (2008) 8910.
- [12] S. Horiuchi, R. Kumai, Y. Tokura, *Adv. Mater.* 23 (2011) 2098.
- [13] S. Horiuchi, Y. Tokumaga, G. Giovannetti, S. Picozzi, H. Itoh, R. Shimano, R. Kumai, Y. Tokura, *Nature* 463 (2010) 789.
- [14] D.A. Kunkel, J. Hooper, S. Simpson, G.A. Rojas, S. Ducharme, T. Usher, E. Zurek, A. Enders, *Phys. Rev. B* 87 (2013) 041402(R).
- [15] K. Zhu, R. Bruinsma, T.G. Mason, *Phys. Rev. B* 3 (2012) 801.
- [16] S.P. Carmichael, M.S. Shell, *J. Chem. Phys.* 139 (2013) 164705.
- [17] G. te Velde, F.M. Bickelhaupt, E.J. Baerends, C. Fonseca Guerra, S.J.A. van Gisbergen, J. G. Snijders, T. Ziegler, *J. Comput. Chem.* 22 (2001) 931.
- [18] E.J. Baerends, J. Autschbach, A. Bérces, F.M. Bickelhaupt, C. Bo, P.M. Boerrigter, L. Cavallo, D.P. Chong, L. Deng, R.M. Dickson, et al., *ADF 2010, scm*, <http://www.scm.com> 2010.
- [19] S. Grimme, J. Antony, S. Ehrlich, H. Krieg, *J. Chem. Phys.* 132 (2010) 154104.
- [20] J.P. Perdew, K. Burke, Y. Wang, *Phys. Rev. B* 54 (1996) 16533.
- [21] Y. Zhang, W. Yang, *Phys. Rev. Lett.* 80 (1998) 890.
- [22] J.P. Perdew, K. Burke, M. Ernzerhof, *Phys. Rev. Lett.* 80 (1998) 891.
- [23] B. Hammer, L.B. Hansen, J.K. Norskov, *Phys. Rev. B* 59 (1999) 7413.
- [24] M.D. Hanwell, D.E. Curtis, D. Lonie, T. Vandermeersch, E. Zurek, G.R. Hutchison, *J. Cheminform.* 4 (2012) 1.
- [25] D.C. Lonie, E. Zurek, *Comput. Phys. Commun.* 182 (2011) 2305.
- [26] A. Wach, J. Chen, Z. Falls, D. Lonie, E.R. Mojica, D. Aga, J. Autschbach, *Anal. Chem.* 85 (2013) 8577.
- [27] G. Kresse, J. Hafner, *Phys. Rev. B* 47 (1993) 558.
- [28] P.E. Blöchl, *Phys. Rev. B* 50 (1994) 17953.
- [29] S. Grimme, *J. Comput. Chem.* 27 (2006) 1787.
- [30] K. Lee, E.D. Murray, L. Kong, B.I. Lundqvist, D.C. Langreth, *Phys. Rev. B* 82 (2010) 081101.
- [31] T. Mochida, S. Matsumiya, A. Izuoka, N. Sato, T. Sugawara, Y. Sugawara, *Acta Crystallogr. C* 48 (1992) 680.
- [32] F. Sily, A.Q. Shaw, M.R. Castell, G.A.D. Briggs, M. Mura, N. Martsinovich, L. Kantorovich, *J. Phys. Chem. C* 112 (30) (2008) 11476.
- [33] M. Mura, F. Sily, V. Burlakov, M.R. Castell, G.A.D. Briggs, L.N. Kantorovich, *Phys. Rev. Lett.* 108 (17) (2012) 176103.
- [34] Y. Wei, S.W. Robey, J.E. Reutt-Robey, *J. Phys. Chem. C* 112 (47) (2008) 18537.
- [35] N. Jiang, Y. Wang, Q. Liu, Y. Zhang, Z. Deng, K.-H. Ernst, H.-J. Gao, *Phys. Chem. Chem. Phys.* 12 (2010) 1318.
- [36] Y. Yingchun, W. Sun, Y. Wang, X. Shao, X. Xu, F. Cheng, J. Li, K. Wu, *J. Chem. Phys. Lett.* 111 (2007) 10138.
- [37] J.A. Theobald, N.S. Oxtoby, M.A. Phillips, N.R. Champness, P.H. Beton, *Nature* 424 (2003) 1029.
- [38] M. Ruben, D. Payer, A. Landa, A. Comisso, C. Gattinoni, N. Lin, J.-P. Collin, J.-P. Sauvage, A. De Vita, K. Kern, *J. Am. Chem. Soc.* 128 (2006) 15644.
- [39] D. Kunkel, S. Simpson, J. Nitz, G. Rojas, E. Zurek, L. Routaboul, B. Doudin, P. Braunstein, P. Dowben, A. Eders, *Chem. Commun.* 48 (2012) 7143.
- [40] S. Simpson, E. Zurek, *J. Phys. Chem. C* 116 (2012) 12636.
- [41] G. Rojas, S. Simpson, X. Chen, D. Kunkel, J. Nitz, J. Xiao, P.A. Dowben, E. Zurek, A. Enders, *Phys. Chem. Chem. Phys.* 14 (2012) 4971.
- [42] H. Ishii, K. Sugiyama, E. Ito, K. Seki, *Adv. Mater.* 11 (1999) 605.
- [43] P.S. Bagus, V. Staemmler, C. Wöll, *Phys. Rev. Lett.* 89 (2002) 096104.
- [44] T.K. Haxton, H. Zhou, I. Tambllyn, D. Eom, Z. Hu, J.B. Neaton, T.F. Heinz, S. Whitelam, *Phys. Rev. Lett.* 111 (2013) 265701.
- [45] G. van Anders, N. Khalid Ahmed, R. Smith, M. Engel, S.C. Glotzer, *ACS Nano* 8 (2014) 931.
- [46] S. Simpson, D.A. Kunkel, J. Hooper, J. Nitz, P.A. Dowben, L. Routaboul, P. Braunstein, B. Doudin, A. Enders, E. Zurek, *J. Phys. Chem. C* 117 (2013) 2982.